The direct observations of large aerosol radiative forcing in the Himalayan region

M. V. Ramana, V. Ramanathan, and I. A. Podgorny

Center for Atmospheric Sciences, Scripps Institution of Oceanography, University of California at San Diego, La Jolla, California, USA

Bidya B. Pradhan and Basanta Shrestha

Mountain Environment and Natural Resources Information system, International Centre for Integrated Mountain Development (ICIMOD), Kathmandu, Nepal

Received 11 October 2003; revised 14 January 2004; accepted 4 February 2004; published 6 March 2004.

[1] We show here that absorbing aerosols have led to a large reduction of surface solar radiation during winter over the Himalayan region. Our results are based on radiometric, aerosol and Lidar observations made at three sites in Nepal during winter 2003. The monthly mean aerosol optical depth (AOD) ranged from 0.2 to 0.34 and the TERRA satellite MODIS data reveal that AODs measured over these sites were typical of the entire Himalayan region. The near-surface aerosol single scattering albedo was in the range from 0.7 to 0.9. The presence of strongly absorbing aerosols resulted in a relatively large diurnal mean aerosol surface radiative forcing efficiency of -73 Wm^{-2} (per unit optical depth). The seasonal mean reduction in solar flux was as high as 25 Wm^{-2} and aerosol heating as much as 1 K per day within the first two kilometers. *INDEX TERMS:* 0305 Atmospheric Composition and Structure: Aerosols and particles (0345, 4801); 0345 Atmospheric Composition and Structure: Pollution—urban and regional (0305); 4801 Oceanography: Biological and Chemical: Aerosols (0305); 0360 Atmospheric Composition and Structure: Transmission and scattering of radiation; 1610 Global Change: Atmosphere (0315, 0325); 1803 Hydrology: Anthropogenic effects. **Citation:** Ramana, M. V., V. Ramanathan, I. A. Podgorny, B. B. Pradhan, and B. Shrestha (2004), The direct observations of large aerosol radiative forcing in the Himalayan region, *Geophys. Res. Lett.*, *31*, L05111, doi:10.1029/2003GL018824.

1. Introduction

[2] The Atmospheric Brown Cloud (ABC) project is an international research effort initiated by the United Nations Environment Programme (UNEP) and its current focus is on the Asia region [*Ramanathan and Crutzen*, 2003]. The project seeks to answer the major environmental challenges facing the Indo-Asia-Pacific region in the coming decades, specifically the environmental consequences of rising air pollution levels due to rapid industrialization and population growth. The ABC is built upon the Indian Ocean Experiment (INDOEX) completed in 1998–1999 [*Ramanathan et al.*, 2001a].

[3] While INDOEX was mostly focused on the pollution outflow from the Indian subcontinent to the Indian Ocean during winter monsoon, the ABC project will have a much broader scope. In particular, one of the prospective stationary observational sites will be located in the Himalayan region. As shown during INDOEX [*Ramanathan et al.*, 2001a; *Leon et al.*, 2001; *Muller et al.*, 2001; *de Reus et al.*, 2001], this region is subject to a heavy loading of aerosols during the winter season (see Figure 1). As seen from Figure 1, this region provides an excellent setting for studying the radiative forcing effects of anthropogenic aerosols in South Asia. Towards this goal, the first direct observations of aerosol radiative forcing have been carried out in winter 2003 in Nepal. The objective of the paper is manifold. First, we need to quantify the magnitude of aerosol forcing which has direct implications for estimating the complex effects of pollution on the regional climate and hydrological cycle [*Ramanathan et al.*, 2001b]. Secondly, the results of the paper will be instrumental in defining the ABC observational strategy in the Himalayan region. Finally, in situ aerosol and radiometric observation will help validate the regional aerosol forcing estimates based on satellite measurements [e.g., *Kaufman et al.*, 2002, and references therein].

2. Experimental Setup

[4] The data presented have been collected during winter 2003 at Kathmandu (27.67°N, 85.31°E, elevation −1350 m), the capital of Nepal; Godavari (27.59°N, 85.31°E, elevation −1600 m), a more remote location about 10 km south of Kathmandu; and Nagarkot (27.71°N, 85.52°E, elevation −1975 m), a remote hilly site above the Kathmandu valley 32 km east of Kathmandu. The directly measured aerosol and radiometric quantities included aerosol optical depth (AOD), aerosol single scattering albedo (SSA), aerosol vertical profile and global broadband shortwave fluxes at the surface. Microtops sunphotometers have been used at Kathmandu and Nagarkot locations to measure AOD at 340, 440, 500, 675, 870 and 1020 nm, total columnar water and ozone.

[5] The Radiance Research portable M903 Nephelometer and Particle Soot Absorption Photometer (PSAP) have been used at the Godavari site to measure the near-real-time aerosol scattering and absorption coefficients at 550 nm, respectively. SSA (the ratio of the aerosol scattering coefficient to the total aerosol extinction coefficient) has been computed from the simultaneous measurements of aerosol scattering and absorption coefficients. PSAP data have been processed following *Bond et al.* [1999].

0094-8276/04/2003GL018824$05.00

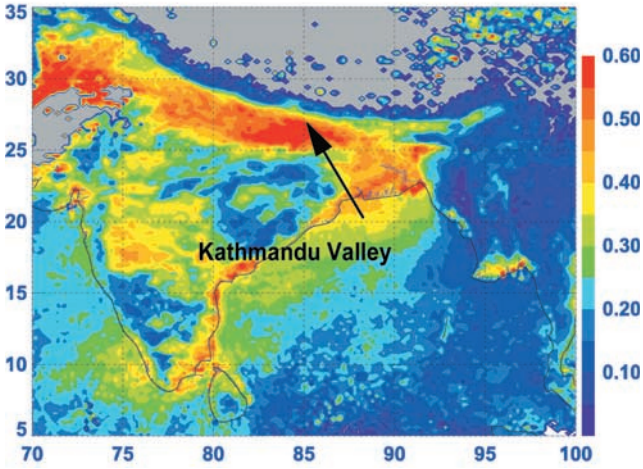

Figure 1. Regional distribution of natural and anthropogenic aerosol optical depth at 0.55 μm derived from Moderate Resolution Imaging Spectroradiometer (MODIS) instrument onboard the Terra satellite (December 2002).

[6] For the first time, Lidar observations of tropospheric aerosols have been carried out in the Himalayan region using a high-resolution (0.030 km) Micro-Pulse Lidar (MPL) system [*Spinhirne et al.*, 1995]. MPL has been installed inside a climate-controlled housing at Kathmandu site and operated continuously during February 9–17, 2003 at 523 nm. The MPL signals have been averaged and stored at 1-min time intervals up to the altitude of 30 km and have been processed following *Campbell et al.* [2002]. The Microtops AODs at 523 nm have been used to calibrate the MPL. The aerosol extinction profile has been determined following *Welton et al.* [2000].

[7] Finally, CM21 Kipp & Zonen ventilated pyranometers have been used at Kathmandu (Jan. 7 to Feb. 17, 2003) and Nagarkot (Feb. 10 to Mar. 30, 2003) sites to obtain broadband (280–2800 nm) global radiative fluxes at the surface. The pyranometer absolute accuracy is ±9 Wm^{-2} and the error due to directional response is about ±10 Wm^{-2}. Pyranometers and Microtops have been purchased just before the start of this study and calibrated at Kipp & Zonen and Solar Light Co. respectively.

3. Results

3.1. Observed Aerosol Characteristics

[8] Shown in Figure 2a are variations of daily mean AOD at 500 nm at the Kathmandu (0.16 to 0.55 ranges) and Nagarkot (0.06 to 0.29 ranges) sites in winter 2003. The average clear sky AOD value at Kathmandu is 0.34, which is typical for the polluted areas. The Angstrom coefficients have been determined by calculation, on a logarithm scale, the linear-square-fit slope of the spectral sunphotometer measurements (340–1020 nm) as a function of wavelength. The mean value of the Angstrom exponent during the observational campaign was 1.3 and 1.4 at the Kathmandu and Nagarkot sites respectively, pointing out the dominance of sub-micron aerosol particles at both sites.

[9] Monthly mean (January 7 to February 17, 2003) SSAs measured under ambient conditions at Godavari are shown in Figure 2b as a function of time of the day. As seen from Figure 2b, SSA values exhibit a diurnal cycle ranging from 0.7 to 0.9. The diurnal cycle in aerosol SSA is most likely due to RH, which varied from a low of about 55% (±12%) during local noon to a high of about 72% (±10%) during the night. The time of low and high values of SSA in Figure 2b coincide approximately with the times of the observed low and high values of RH. The positive correlation between SSA and RH is due to the growth of aerosols with humidity which enhances the scattering.

[10] Figure 3 shows 24-hour averaged vertical aerosol extinction profile from the MPL on Feb. 10, 2003. 24-hour average profile is calculated using the profiles derived from each 30-min MPL averages. The extinction profile showed a decrease in extinction from the surface to near 0.3 km, followed by extinction minimum at 0.3–0.6 km. Extinction then increased with altitude up to a mean extinction maximum at 1.3 km, finally decreasing until reaching the top of the aerosol layer, which is near 2.0 km altitude. The layer below 0.3 km is possibly due to aerosols originating locally. The peak seen at ~1.3 km above ground level (~2.6 km MSL) is most likely due to dry convective lifting of pollutants at distant sources and subsequent horizontal upper air long- range transport. It is important to note from Figure 1 that aerosols over the Kathmandu valley is part of a wide spread layer of aerosols over the entire Indo-Gangetic plains.

3.2. Aerosol Radiative Forcing in the Himalayan Region

[11] In order to ensure that the observed solar fluxes are consistent with measured aerosol properties (Figures 2a to 3), we used the Monte Carlo Radiative Transfer model described in *Podgorny et al.* [2000] and compare observed

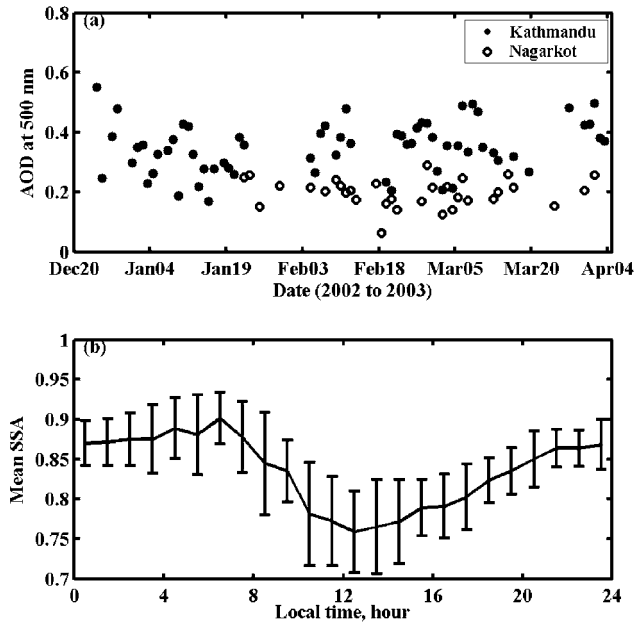

Figure 2. (a) Temporal variation of daily mean aerosol optical depth (AOD) at 500 nm at the Kathmandu and Nagarkot sites during the observational campaign; (b) Diurnal cycle of monthly mean aerosol single scattering albedo (SSA) at the Godavari site during January–February 2003. The vertical bars represent standard deviations.

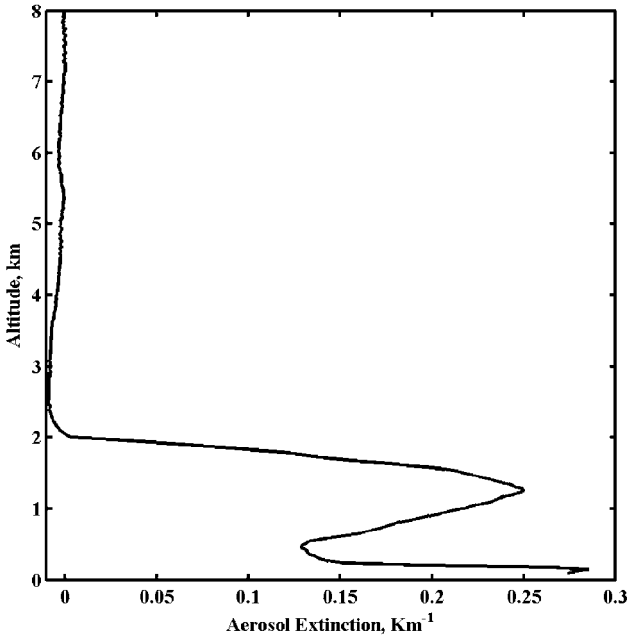

Figure 3. 24-hour average aerosol extinction profile at the Kathmandu site on a clear day February 10, 2003. The ordinate represents height above the ground surface, which is ~1.3 km above the mean sea level.

with model computed fluxes. We could do this comparison only for the Kathmandu site. The number of usable observations at Nagarkot were too few to permit statistically significant comparisons. The INDOEX aerosol model [*Satheesh et al.*, 1999] is used as input for the Monte Carlo calculations; however, certain adjustments are made to account for the local conditions. Specifically, (1) dust and sea salt contributions are assigned to be zero, (2) soluble species contributions are rescaled to account for the observed relative humidity, and (3) soot contribution is rescaled to match the observed SSA at Godavari. The measured AOD, column water and ozone from Microtops measurements and vertical extinction distribution from Lidar observations are used as inputs into the model. During the Monte Carlo integration, the effect of Himalayas has been simulated by blocking the photons from 5° elevations to the north of both sites. The clear sky screening of the measured fluxes was done following the procedure described in *Satheesh et al.* [1999] and *Conant* [2000]. Fog typically persists till mid-morning over the Kathmandu valley; therefore radiometric data prior to this period was not used for the analysis. The solar zenith angle was limited to less than 60° to avoid the shading affect from the hills and mountains. These constraints confine the data used in this study to a local time period of 11 to 15 hrs; during this interval, the measured average SSA (see Figure 2b) was 0.78 for clear sky conditions. We assumed that the surface SSA is valid for the entire column. Figure 4 compares broadband (280–2800 nm) observed global radiation fluxes with calculated fluxes for the Kathmandu site. The model overestimates measured fluxes by 5.2 Wm^{-2} with root mean square (RMS) error of 5.3 Wm^{-2}. These differences, however, are well within instrumental uncertainty and similar differences [*Markowicz et al.*, 2002; *Conant*, 2000; *Satheesh et al.*, 1999] were documented previously.

[12] The aerosol radiative forcing at the surface is the effect of aerosol, both natural and anthropogenic, on the net short-wave radiative fluxes and is defined as the difference between the observed clear-sky net shortwave radiative flux and the net shortwave radiative flux for the aerosol-free atmosphere. We employ the two independent methods described in *Satheesh and Ramanathan* [2000] for obtaining aerosol shortwave radiative forcing directly from the observed fluxes. The first method relies solely on observations to derive the forcing efficiency. The second method employs a combination of models (for aerosol-free fluxes) and observations.

[13] ***First method:*** We construct a reference diurnal cycle by fitting a polynomial curve to the screened clear-sky data. We then normalize all of the observed fluxes to this diurnal cycle to convert the instantaneous values to equivalent 24-hour average fluxes. To calculate the net fluxes (down minus up) we assumed that the broadband surface albedo was 0.20 [*Briegleb et al.*, 1986]. The resulting 24-hour average net flux is plotted against corresponding AOD as shown in Figure 5a. The slope of the 24-hour average net flux versus AOD yields the aerosol surface forcing efficiency. We derive the aerosol surface forcing efficiency over Kathmandu for January and February to be -76 Wm^{-2} and -73 Wm^{-2} respectively.

[14] ***Second method:*** In this method, we first estimate the daily mean aerosol forcing and obtain the efficiency by plotting the forcing versus AOD. The diurnal aerosol radiative forcing is obtained by subtracting the observed diurnal solar flux from that estimated by the model for an aerosol-free atmosphere. The 24-hour average aerosol radiative forcing using the above approach is shown in Figure 5b as a function of AOD at 500 nm. The 24-hour average aerosol forcing efficiency was found to be -73 Wm^{-2} at the Kathmandu site. Both the approaches for obtaining forcing efficiency yield similar estimates.

[15] The aerosol optical depth, which when multiplied with forcing efficiency yields the 24-hour average aerosol forcing. The diurnally averaged surface aerosol forcing at Kathmandu (1.35 km above MSL) is about -25 Wm^{-2} for an optical depth of 0.34 at 500 nm. The top of the atmospheric (TOA) forcing estimated by the model is about zero (about -0.2 Wm^{-2}), and since the TOA forcing is the sum of the surface forcing and the atmospheric forcing, the atmospheric forcing is inferred to be +25 Wm^{-2}. Further-

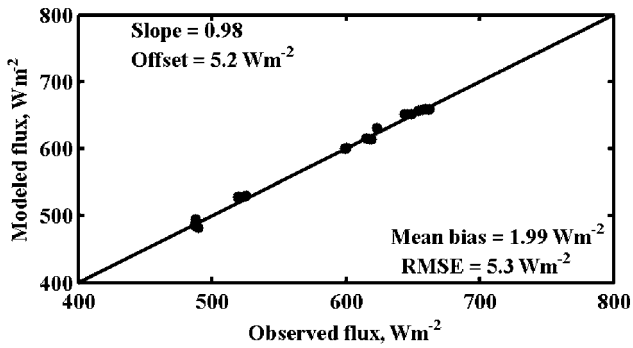

Figure 4. Observed versus modeled surface broadband (280–2800 nm) global fluxes at the Kathmandu site. The solid line corresponds to perfect agreement.

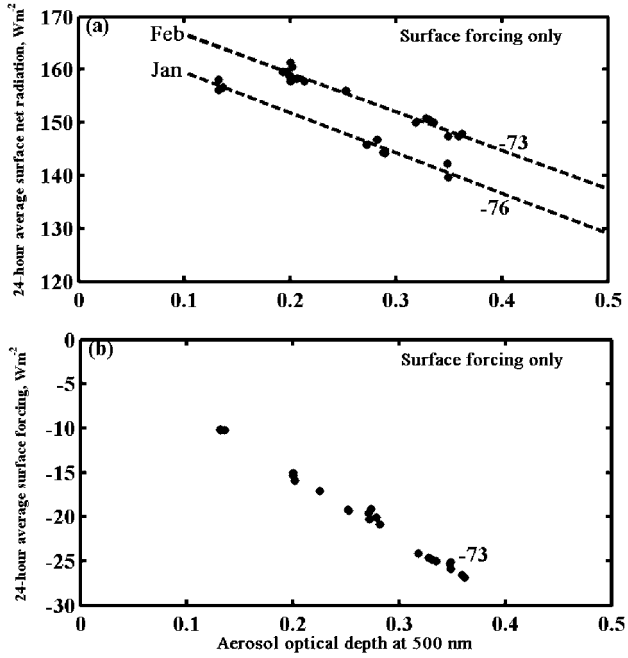

Figure 5. Aerosol radiative forcing efficiency at the surface employing two independent methods: (a) 24-hour average net radiation at the surface as a function of AOD at Kathmandu, (b) 24-hour average aerosol broadband (280–2800 nm) radiative forcing at the surface as a function of AOD at the Kathmandu site. The 24-hour average aerosol forcing efficiency is obtained as the best linear fit to the aerosol forcing values.

more, since the aerosol is largely confined to the first 2 kilometers (see Figure 3), the atmospheric forcing of 25 Wm^{-2} translates into a heating rate of about 1 k/day between the surface and 2 km.

4. Conclusions

[16] Aerosol visible optical depths over the Himalayan region are as high as 0.6 and aerosol single scattering albedo are as low as 0.78 indicating the presence of significant amount of absorbing aerosols. As far as the regional significance of the present results are concerned, the large values of aerosol optical depth, Angstrom wavelength exponent and low values of aerosol single scattering albedo over the Himalayas and the wide spread nature of the pollution (see Figure 1) indicates the importance of anthropogenic aerosols. The presence of aerosols over this region decreased the mean clear-sky radiation observed at the surface by as much as 25 Wm^{-2}. The aerosol radiative forcing over Himalayas is as high as compared to other polluted regions in the world [*Jayaraman et al.*, 1998; *Kaufman et al.*, 2002; *Markowicz et al.*, 2002; *Ramanathan et al.*, 2001a; *Russell et al.*, 1999]. The inferred short wave atmospheric forcing of 25 Wm^{-2} and the heating rate of 1 K/day within the first two kilometers should have a large impact on the winter time inversion and aerosol residence time over this region.

[17] **Acknowledgments.** National Science Foundation Award #0201946 and National Atmospheric and Oceanic Administration Award # NA17RJ1231 supported this research. Authors thank Mr. S. Shrestha of UNEP-Bangkok office for coordinating this experiment with Nepal Government. We also thank ICIMOD for assisting with measurements at the Kathmandu and Nagarkot sites, A. Vogelmann for helpful discussions and F. Li for his help in preparing Figure 1. We wish to thank two anonymous reviewers who provided useful comments.

References

Bond, T. C., T. L. Anderson, and D. Campbell (1999), Calibration and intercomparison of filter-based measurements of visible light absorption by aerosols, *Aerosol Sci. Technol.*, *30*, 582–600.

Briegleb, B. P., P. Minnis, V. Ramanathan, and E. Harrison (1986), Comparison of Regional Clear-Sky Albedos Inferred from Satellite Observations and Model Computations, *J. Clim. Appl. Meteorol.*, *25*, 214–226.

Campbell, J. R., D. L. Hlavka, E. J. Welton, C. J. Flynn, D. D. Turner, J. D. Spinhirne, V. S. Scott, and I. H. Hwang (2002), Full-time, eye-safe cloud and aerosol lidar observation at Atmospheric Radiation Measurement Program sites: Instrument and data processing, *J. Atmos. Oceanic Technol.*, *19*, 431–442.

Conant, W. C. (2000), An observational approach for determining aerosol surface radiative forcing: Results from the first field phase of INDOEX, *J. Geophys. Res.*, *105*(D12), 15,347–15,360.

de Reus, M., R. Krejci, J. Williams, H. Fischer, R. Scheele, and J. Strom (2001), Vertical and horizontal distribution of the aerosol number concentration and size distribution over the northern Indian Ocean, *J. Geophys. Res.*, *106*(D22), 28,629–28,641.

Jayaraman, A., D. Lubin, S. Ramachandran, V. Ramanathan, E. Woodbridge, W. D. Collins, and K. S. Zalpuri (1998), Direct observations of aerosol radiative forcing over the tropical Indian Ocean during the January-February 1996 pre-INDOEX cruise, *J. Geophys. Res.*, *103*(D12), 13,827–13,836.

Leon, J.-F., et al. (2001), Large-scale advection of continental aerosols during INDOEX, *J. Geophys. Res.*, *106*(D22), 28,427–28,439.

Kaufman, Y. J., D. Tanre, and O. Boucher (2002), A sattelite view of aerosols in the climate system, *Nature*, *419*, 215–223.

Markowicz, K. M., P. J. Flatau, M. V. Ramana, P. J. Crutzen, and V. Ramanathan (2002), Absorbing Mediterranean aerosols lead to a large reduction in the solar radiation at the surface, *Geophys. Res. Lett.*, *29*(20), 1968, doi:10.1029/2002GL015767.

Muller, D., K. Franke, F. Wagner, D. Althausen, A. Ansmann, and J. Heintzenberg (2001), Vertical profiling of optical and physical particle properties over the tropical Indian Ocean with six-wavelength lidar 1. Seasonal cycle, *J. Geophys. Res.*, *106*(D22), 28,567–28,575.

Podgorny, I. A., W. C. Conant, V. Ramanathan, and S. K. Satheesh (2000), Aerosol modulation of atmospheric and solar heating over the tropical Indian Ocean, *Tellus*, *52B*, 947–958.

Ramanathan, V., and P. J. Crutzen (2003), New Directions: Atmospheric Brown Clouds, *Atmos. Environ.*, *37*, 4033–4035.

Ramanathan, V., et al. (2001a), The Indian Ocean Experiment: An integrated analysis of the climate forcing and effects of the Great Indo-Asian Haze, *J. Geophys. Res.*, *106*(D22), 28,371–28,398.

Ramanathan, V., P. J. Crutzen, J. T. Kiehl, and D. Rosenfeld (2001b), Aerosols, climate, and the hydrological cycle, *Science*, *294*, 2119–2124.

Russell, P. B., J. M. Livingston, P. Hignett, S. Kinne, J. Wong, A. Chien, R. Bergstrom, P. Durkee, and P. V. Hobbs (1999), Aerosol-induced radiative flux changes off the United Sates mid-Atlantic coast: Comparison of values calculated from sunphotometer and in situ data with those measured by airborne pyranometer, *J. Geophys. Res.*, *104*(D2), 2289–2307.

Satheesh, S. K., V. Ramanathan, Xu Li-Jones, J. M. Lobert, I. A. Podgorny, J. M. Prospero, B. N. Holben, and N. G. Loeb (1999), A model for the natural and antropogenic aerosols over the tropical Indian Ocean derived from Indian Ocean Experiment data, *J. Geophys. Res.*, *104*(D22), 27,421–27,440.

Satheesh, S. K., and V. Ramanathan (2000), Large differences in tropical aerosol forcing at the top of the atmosphere and Earth's surface, *Nature*, *405*, 60–63.

Spinhirne, J. D., J. Rall, and V. S. Scott (1995), Compact eye-safe lidar systems, *Rev. Laser Eng.*, *23*, 26–32.

Welton, E. J., et al. (2000), Ground-based Lidar Measurements of Aerosols during ACE-2: Instrument description, Results, and comparisons with other ground-based and airborne measurements, *Tellus*, *52B*, 635–650.

M. V. Ramana, V. Ramanathan, and I. A. Podgorny, Center for Atmospheric Sciences, Scripps Institution of Oceanography, University of California at San Diego, La Jolla, CA 92093-0221, USA. (ramana@fiji.ucsd.edu)

B. B. Pradhan and B. Shrestha, Mountain Environment and Natural Resources Information system, International Centre for Integrated Mountain Development (ICIMOD), Kathmandu, Nepal.